25–29 July, 2004 • Budapest, Hungary

# Takagi–Sugeno Fuzzy Gain Scheduling with Sampling-Time Uncertainties

Bourhane Kadmiry
Department of Computer Sc. (AIICS)
Linköping University
Linköping SE-581 83
E-mail: bouka@ida.liu.se

Dimiter Driankov
Departement of Technology (AASS)
Örebro University
Örebro SE-701 82
E-mail: dimdr@ida.liu.se

***Abstract*— This paper addresses the robust fuzzy control problem for discrete-time nonlinear systems in the presence of sampling time uncertainties. The case of the discrete T–S fuzzy system with sampling-time uncertainty is considered and a robust controller design method is proposed. The sufficient conditions and the design procedure are formulated in the form of linear matrix inequalities (LMI). The effectiveness of the proposed controller design methodology is demonstrated of a visual-servoing control problem.**

## I. INTRODUCTION

Robustness in fuzzy model-based control in *discrete-time models with fixed sampling-time* and parametric uncertainties has been studied before [1]. *Asymptotic stability for Takagi–Sugeno (T–S) fuzzy system with fixed and known time-delays* was addressed for both the continuous- and discrete-time cases in [2]. *Augmented stability with guaranteed-cost* design for T–S fuzzy controllers in discrete-time case with fixed sampling-time is presented in [3]. Our novel contribution in this work is to reflect these approaches altogether into a scheme to tackle the problem of *uncertainty due to varying sampling-time in the discrete-time case*. The idea that the system is described as a combination of locally linear sub-models where the varying sampling-time is a used as a gain scheduled parameter motivates the FGS approach and LMIs-based performance analysis.

In the following pages, section II addresses the discrete-time model and its T–S form using the FGS approach. Section III presents the controller design method for robust stabilization in discrete-time of the T–S fuzzy systems in the presence of varying sampling-time. Section IV illustrate an application for the use of the control method proposed, and section V shows controller design feasibility and simulation results.

## II. T-S FUZZY MODEL

The discrete-time model considered is of the form

$$\begin{aligned} x_{k+1} &= Gx_k + H(x_k)u_k \\ &= x_k + \tau B(x_k)u_k \end{aligned} \tag{1}$$

where $G$ is the identity matrix $I$, and $H$ is the discrete Euler approximation depending on the state variable $x_k$, the varying sampling-time $\tau$, and is expressed as $H = \tau B$ where $B$ is the control matrix in the continuous-time case. Uncertainties may originate from the model parameters, or disturbances in the state. We are aware of these uncertainties but, cannot give an explicit quantification of them. Thus the resulting uncertain system will be reduced to its varying sampling-time description. Then the T–S version of the discrete-time model in (1) develops as follows

$$\begin{aligned} x_{k+1} &= \sum_{i=1}^{r} w_i(z_k)(x_k + \tau B_i u_k), \\ \tau &\in [\tau_{min}, \tau_{max}];\ x_k \in [x_{min}, x_{max}] \end{aligned} \tag{2}$$

where $z_k = [x_k, \tau]$ is the vector of scheduled variables, and $r$ is the number of rules. $w_i(z_k)$ are the weights given as combination of $s$ membership functions $F_s$ in the IF-part of the rules [4], given a particular value of $z_k$, and expressed as

$$w_k = \frac{\prod_{i=1}^{s} F_i(z_k)}{\sum_{i=1}^{r} w_i(z_k)} \tag{3}$$

The system (2) is obtained from a fuzzy rule base where a rule $r$ is of the form

$$\begin{aligned} r:\ &\text{IF } z \text{ is } F_1 \text{ and } \cdots \text{ and } z \text{ is } F_s \\ &\text{THEN } x_{k+1} = x_k + \tau B_r u_k \end{aligned} \tag{4}$$

In order to cope with the uncertainty in sampling time, the control matrix H from (1) is represented in the discrete-time version of the rule (4), which is expanded into two rules, as: $H_r = \tau_{min} B_r$ for $r_{min}$ and $H_r = \tau_{max} B_r$ for $r_{max}$. This increase the number of rules to $2r$, and this transformation will –by convexity arguments– guarantee that the system is robust with respect to the varying sampling-time. Each rule $r$ will be expanded as follows

$$\begin{aligned} r_{min}:\ &\text{IF } z \text{ is } F_1 \text{ and } \cdots \text{ and } z \text{ is } F_s \text{ and } \tau \text{ is } \tau_{min} \\ &\text{THEN } x_{k+1} = x_k + \tau_{min} B_r u_k \\ r_{max}:\ &\text{IF } z \text{ is } F_1 \text{ and } \cdots \text{ and } z \text{ is } F_s \text{ and } \tau \text{ is } \tau_{max} \\ &\text{THEN } x_{k+1} = x_k + \tau_{max} B_r u_k \end{aligned} \tag{5}$$

The next step in the control design will be to develop the closed-loop system in a T–S form.

0-7803-8353-2/04/$20.00 © 2004 IEEE

## III. FGS CONTROL DESIGN

This section presents a fuzzy gain scheduled state-feedback controller for the system in (2), which is of the form

$$u_k = -K(z_k)x_k = -\sum_{r=1}^{8} w_r(z_k)K_r x_k \tag{6}$$

where the weights $w_r(z_k)$ are the ones used for the model description in (3). The closed-loop develops as

$$x_{k+1} = \sum_{i=1}^{8}\sum_{j=1}^{8} w_i(z_k)w_j(z_k)[I - \tau B_i K_j]x_k \tag{7}$$

Notice that the control matrix $B_i$ and the control gain matrix $K_j$ differ for each region described by a rule $r$. In this case, each one of the rules $r_{min}$ and $r_{max}$ in (5) will be written as follows

$r_{min}$ : IF $z$ is $F_1$ and $\cdots$ and $z$ is $F_s$ and $\tau$ is $\tau_{min}$
THEN $x_{k+1} = (I - \tau_{min}B_r K_r)x_k$

$r_{max}$ : IF $z$ is $F_1$ and $\cdots$ and $z$ is $F_s$ and $\tau$ is $\tau_{max}$
THEN $x_{k+1} = (I - \tau_{max}B_r Kr)x_k$

Notice that, in both the rules $r_{min}$ and $r_{max}$, the gain $K_r$ is the same.The objective of the control design is to compute the feedback gains $K_j, (j = 1..8)$, so that

- the closed-loop system in (7) is asymptotically stable w.r.t sampling-time uncertainty.
- the closed loop system in (7) has a guaranteed $H_2$ performance.

Asymptotic stability and guaranteed-cost will be developed in the next sections

### A. Asymptotic stability using LMIs

The closed-loop fuzzy system (7) is globally asymptotically stable, if there exist a positive-definite matrix $P$ which satisfies the following Lyapunov inequality [2]

$$\begin{aligned}&(G - HK)^T P(G - HK) - P = 0;\\ &K = XP\end{aligned} \tag{8}$$

where $X \geq 0$. Pre- and post-multiplying both sides of (8) by $P^{-1}$ and using the change of variables $Y = P^{-1}$ and $X_i = K_i Y$ we obtain a set of quadratic inequalities. For easing the annotations we define the matrices $N_{ik}$ and $O_{ijk}$ as follows

$$\begin{aligned}N_{ik} &= G_i Y - \tau_k B_i K_i Y = I_2 - \tau_k B_i X_i;\\ O_{ijk} &= (G_i + G_j)Y - (\tau_k B_i K_j + \tau_k B_j K_i)Y\\ &= 2I_2 - \tau_k B_i X_j - \tau_k B_j X_i\end{aligned} \tag{9}$$

The system described in (8) can be transformed into LMIs as follows

$$\begin{aligned}&Y > 0; \quad i = 1..8, j < i \leq 8, k = 1..2\\ &\begin{bmatrix} Y & N_{ik}^T \\ N_{ik} & Y \end{bmatrix} > 0;\\ &\begin{bmatrix} Y & O_{ijk}^T \\ O_{ijk} & Y \end{bmatrix} > 0\end{aligned} \tag{10}$$

If the above LMIs have a common positive definite solution, stability is guaranteed. But stability in most of physical problems is not enough by itself most of the time, since the control has to satisfy certain design objectives. This will be addressed in the following section.

### B. Optimal $H_2$ cost design

The discrete-time performance for a fixed and known time-delay has been discussed in [2]. Optimal $H_2$ cost for discrete-time T–S without delays is presented in [3]. In this section, we combine these results for the discrete-time case with varying sampling-time. We show that the problem of minimizing an upper bound on a quadratic performance measure can be recast as a trace minimization problem. This is done subject to a set LMIs , which guarantees that the quadratic cost of the system would not exceed a specified limit. To achieve guaranteed $H_2$ performance, the following cost function is minimized

$$J = \sum_{j=1}^{\infty} x_k^T Q x_k + u_k^T R u_k \tag{11}$$

subject to (2) and (6). This is the common LQR cost-function used in linear optimal control. The closed-loop fuzzy system (7) has a $H_2$ performance with a guaranteed cost if there exist a positive-definite matrix $P$ which satisfies the following Lyapunov inequality (8) augmented with the cost function [3].

$$\begin{aligned}&(G - HK)^T P(G - HK) - P + Q + K^T RK = 0;\\ &K = R^{-1}H^T P\end{aligned}$$

where $Q \geq 0$ and $R \geq 0$. Minimizing the cost function results in finding the positive-definite matrix $P$, solution of the Lyapunov equation (8). The solution of the optimal cost problem is dealt using the LMI approach by solving the following optimization problem

**Min tr(Z) Subject to**

$$\begin{aligned}&i = 1..8, j < i \leq 8, k = 1..2\\ &\begin{bmatrix} Z & I_2 \\ I_2 & Y \end{bmatrix} > 0;\\ &\begin{bmatrix} Y & N_{ik}^T & YQ^{\frac{1}{2}} & X_1^T R^{\frac{1}{2}} & \dots & X_8^T R^{\frac{1}{2}} \\ N_{ik} & Y & 0 & 0 & \dots & 0 \\ Q^{\frac{1}{2}}Y & 0 & I_2 & 0 & \dots & 0 \\ R^{\frac{1}{2}}X_1 & 0 & 0 & I_2 & \dots & 0 \\ \vdots & \vdots & \vdots & \vdots & \ddots & \vdots \\ R^{\frac{1}{2}}X_8 & 0 & 0 & 0 & \dots & I_2 \end{bmatrix} > 0;\\ &\begin{bmatrix} Y & O_{ijk}^T & YQ^{\frac{1}{2}} & X_1^T R^{\frac{1}{2}} & \dots & X_8^T R^{\frac{1}{2}} \\ O_{ijk} & Y & 0 & 0 & \dots & 0 \\ Q^{\frac{1}{2}}Y & 0 & I_2 & 0 & \dots & 0 \\ R^{\frac{1}{2}}X_1 & 0 & 0 & I_2 & \dots & 0 \\ \vdots & \vdots & \vdots & \vdots & \ddots & \vdots \\ R^{\frac{1}{2}}X_8 & 0 & 0 & 0 & \dots & I_2 \end{bmatrix} > 0\end{aligned} \tag{12}$$

If these LMIs are feasible, we calculate the controller gains as

$$K_r = X_r Y^{-1}, \; r = 1..8 \tag{13}$$

The obtained $K_r$'s insure closed-loop asymptotic stablity w.r.t the varying $\tau$ with guaranteed cost. Once the controller gains in (13) are found, the global T-S controller is obtained using (6).

## IV. Visual-servoing application

### A. General scheme

The global visual-servoing scheme, on which the control design described in section III is implemented, is illustrated in Fig. 1

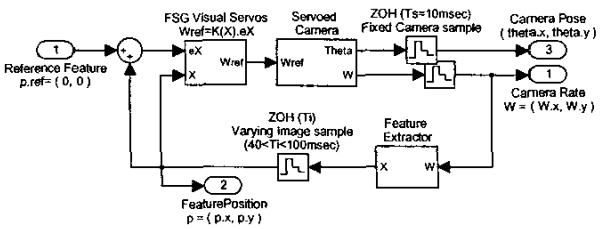


Fig. 1. The visual-servoing scheme

This system functions as follows:

- The camera has its own internal rate and pose controllers. Its inputs are reference values of pan/tilt rates $\omega_x^r$ and $\omega_y^r$. The output of this subsystem is the camera orientation (pose), $\theta_x$ and $\theta_y$, and a video-stream of the region exposed.
- The video-flow is processed by the image-grabber and image-processing subsystem. The image grabber 'samples' the optical flow into separate images (25 images/sec.) which are buffered for further image-processing: Time-delays of varying nature occur at this stage.
- The image-processing inputs the images, and outputs a position $p = [p_x, p_y]$ in image coordinates of a particular feature (see Fig. 2).
- This data is feeded back in real-time to the visual controller. The controller subsystem objective is to position the camera so that the feature is centered in the image (see Fig. 2). It delivers thus a profile of reference values in terms of camera pose-rates to be regulated, in order center the (moving) feature in the image.

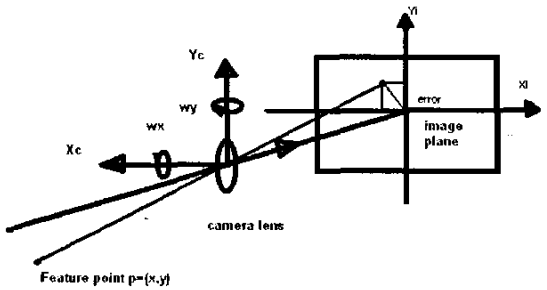


Fig. 2. The control objective

Many factors may be responsible for the degraded stability and performance for the control scheme presented above:

- Time-delays can occur from both the feature extraction process or unknown/unmodelled dynamics of the camera control loop: The performance of the feature extraction process could extend from 40 msec. (video-stream rate), to a 100 msec. (image-processing inherent delays).
- Model parameters, states and un-modelled dynamics may affect the performance: In our setup, the camera –once mounted on the UAV in motion– will see a degradation of its pan/tilt performance due to Coriolis forces induced by the helicopter motion.

Though these conditions affect the performance of the camera, the dynamics induced are not considered for the control design. We only consider the time-sampling uncertainties. The camera and image-processing (CIP) model used [5] is of the form

$$\begin{bmatrix} \dot{p_x} \\ \dot{p_y} \end{bmatrix} = \begin{bmatrix} \frac{p_x p_y}{f} & -\frac{p_x^2+f^2}{f} \\ \frac{p_y^2+f^2}{f} & -\frac{p_x p_y}{f} \end{bmatrix} \begin{bmatrix} \omega_x \\ \omega_y \end{bmatrix} \tag{14}$$

where $\dot{p} = [\dot{p_x}, \dot{p_y}]^T$ is the translational velocity of the feature $p$ in the image frame, and $\omega = [\omega_x, \omega_y]^T$ is the angular velocity of the camera and $f$ is the focal distance for the camera lens. Using the design method described in section III and the method of exact linearization [6], [7], [8], the T–S version of (14) is given as

$$x_{k+1} = \sum_{i=1}^{8}\sum_{j=1}^{8} w_i(z_k)w_j(z_k)[I_2 - \tau B_i K_j]x_k$$

where the weights $w_r(z)$ are computed from the membership functions $F_{nm}^s(z)$ for $s = i, j, k = 1..2$, for a particular value of $z$. Using the expression in (3) we obtain

$$w_r(z) = \frac{F_{11}^i F_{12}^j F_{21}^k}{\sum_{r=1}^{8} w_r(z)} \quad \text{and} \quad \sum_{r=1}^{8} w_r(z) = 1$$

The membership functions $F_{nm}^s(z)$ are derived from the nonlinearities in the matrix $B(x_k)$ in the boundaries $p_x \in [-p_{xm},\ p_{xm}]$, $p_y \in [-p_{ym},\ p_{ym}]$, with ($p_{xm} = 2.210^{-3}m$, $p_{ym} = 1.910^{-3}m$), and are expressed as follows

$$\begin{aligned} F_{11}^1(z) &= \tfrac{1}{2} - \tfrac{p_x p_y}{2p_{xm}p_{ym}}, & F_{11}^2(z) &= 1 - F_{11}^1 \\ F_{12}^1(z) &= \tfrac{p_x^2}{p_{xm}^2}, & F_{12}^2(z) &= 1 - F_{12}^1 \\ F_{21}^1(z) &= 1 - \tfrac{p_y^2}{p_{ym}^2}, & F_{21}^2(z) &= 1 - F_{21}^1 \end{aligned}$$

The fuzzy rules $r$ are then of the form

$$\begin{aligned} r:\ \text{IF } z \text{ is } F_{11}^i \text{ and } z \text{ is } F_{12}^j \text{ and } z \text{ is } F_{21}^k \text{ and } \tau \text{ is } \tau_{min} \\ \text{THEN } x_{k+1} = (I_2 - \tau_{min} B_r K_r)x_k \end{aligned}$$

where the control matrix $B_r$ is expressed in terms of boundaries for the membership functions $F_{nm}^s(z)$ and is of the form

$$B_r = B_{ijk} = \begin{bmatrix} b_{11}^i & b_{12}^j \\ b_{21}^k & -b_{11}^i \end{bmatrix}$$

with

$$b_{11}^1 = -p_{xm}p_{ym}; \quad b_{12}^1 = -f - \frac{p_{xm}^2}{f}; \qquad b_{21}^1 = f;$$

$$b_{11}^2 = \quad p_{xm}p_{ym}; \quad b_{12}^2 = -f; \qquad b_{21}^2 = f + \frac{p_{ym}^2}{f}$$

The graphs illustrating the membership functions $F_{nm}^s$ are shown in Fig. 3.

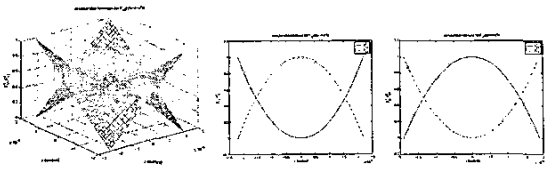

Fig. 3. Membership functions $F_{11}^s$, $F_{12}^s$ and $F_{21}^s$

## V. Simulation and Experiments

In this section, we will illustrate the application of the proposed controller and its performance.

Using the above procedure as described in the previous section, for the given model parameters in terms of image size and focal distance, we perform the design with the following $H_2$ cost parameters $Q$ and $R$ in (11). These parameters are set to: $Q = Diag(10^{-6}, 10^{-6}), R = Diag(10^{-8}, 10^{-8})$. We achieve feasibility of the problem (12), and by minimizing the linear objective, we obtain the P matrix verifying the asymptotic stability and guaranteed-cost robustness

$$P = \begin{bmatrix} 6.94\ 10^{-3} & 5.70\ 10^{-15} \\ 5.70\ 10^{-15} & 7.27\ 10^{-3} \end{bmatrix}$$

We achieve a feasible solution of required accuracy with best objective value: $J = 14\ 10^{-3}$ and $tr(Z) = 14\ 10^{-3}$ Next, we will perform a series of simulations in $Matlab - Simulink$. These simulations are executed comparing the behavior of the system with regards to time-sample variations, for each control channel (pan and tilt). The controllers are implemented in C-language and are used to control the real camera platform as well.

The first simulation is performed for the regulation of position reference values of a point $p$ (image feature), for both sampling times $\tau_{min} = 40$ msec. and $\tau_{max} = 100$ msec. All values of sampling-time within the limits $[\tau_{min}, \tau_{max}]$ show stable behavior. Fig. 4 shows the response by regulation w.r.t $p^d = [0, 0]^T$. The upper-part shows both the error profiles and the camera regulation responses for the x-channel (middle-part) and y-channel (lower-part). The regulation is done for the size of the image. The error is settled to zero after ≈270 msec. for the system sampled at$\tau = 40$ msec., while for the system sampled at $\tau = 100$ msec., the error settles after ≈230 msec. The middle- and lower-parts of Fig. 4 show a step-response for each channel. The system sampled at $\tau_{min}$ has a smoother response, which translates to a camera rotation without *shake*, which in term translates to a settlement without overshoot. The system sampled at $\tau_{max}$ has a dead-beat behavior with

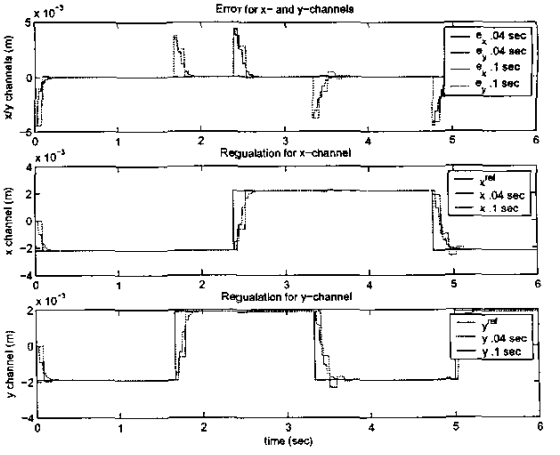


Fig. 4. Comparison between systems sampled at 40 and 100 msec. for regulation

faster response (up to 140 msec. to reach 90% of the reference value) and an overshoot of (≈ 6%).

The second simulation is performed for the tracking of the same feature, for both sampling times $\tau_{min} = 40$ msec. and $\tau_{max} = 100$ msec. with inducing in the reference values an error profile of a sinusoidal shape. Fig. 5 shows both the error profiles (upper-part) and the camera tracking responses for x-channel (middle-part) and y-channel (lower-part). The tracking error presents a saw-teeth shaped oscillation around the sinusoidal shape of the error fluctuation. This oscillation is due to the integration factor that the sampled position undergo in the closed-loop, thus is more pronounced for the time sampling $\tau_{max}$. The oscillation does not appear in the regulation case because of the signal flatness between two reference values. The oscillation is bounded to ≈ 8% of the error amplitude, while the error fluctuation is bounded to ≈ 2% of the amplitude of the tracked profile of reference.

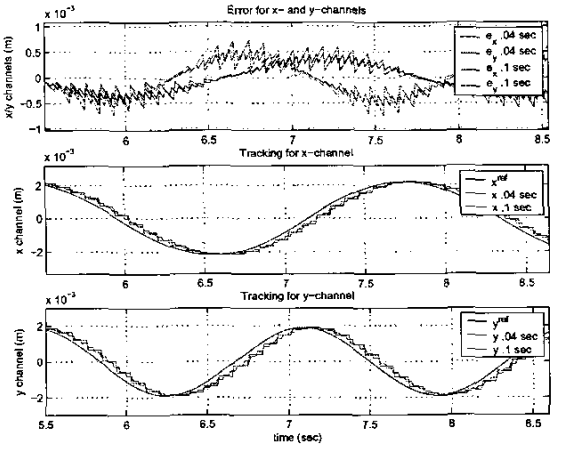


Fig. 5. Comparison between systems sampled at 40 and 100 msec. for tracking

The delays between reference values and output response for the tracking scheme are respectively about 80 msec. for the system sampled at $\tau = 40$ msec. and 70 msec. for the one at $\tau = 100$ msec., that is for both the channels x and y.

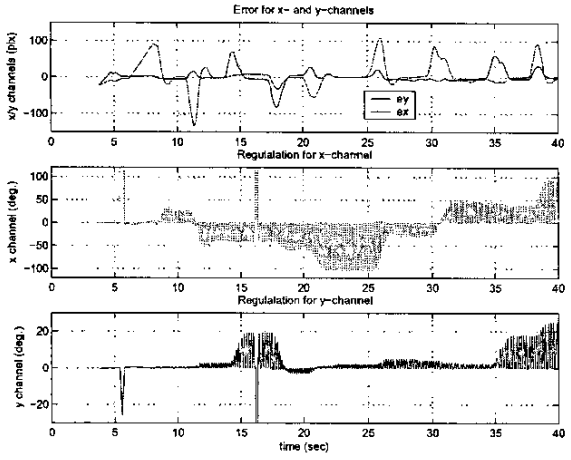


Fig. 6. Camera angles regulation using angular rate control

Third, we run an experiment on the real camera platform, for regulation. Fig. 6 show a scenario in which a beacon whose pattern permits to identify the feature is placed suddenly in the image field of a the camera. The camera is controlled in angular rate control mode, and responds by centering the feature in the image.Fig. 6 shows both the error profiles (upper-part) and the camera pose responses for the x-channel (middle-part) and y-channel (lower-part). The last two profiles in Fig. 6 are in degrees, and these readings are done at sampling time of ≈88 msec. The x-channel presents an overshoot of $\approx 14\%$, with a time response of $\approx 1.3$ sec. for both channels.The profiles show overshoots for both the x- and y-channels; this occurs mainly due to coupling between the two channels. The time responses for the real platform are longer than this of simulation model. This is due to the camera DC-motor closed-loop dynamics, which are not taken into account in the model used for simulation.

Last, we proceed similarly as experiment 3, with moving the camera over the pattern, or moving the pattern in front of the camera. This results in a profile tracking scheme whose results are illustrated in Fig. 7. Both the error profiles for the x- and y-channels are shown in the upper-part of Fig. 7, and the camera pose responses for the x-channel (middle-part) and y-channel (lower-part) illustrate the rotation of the camera in pan and tilt in order to center the feature in the image. The amplitude of the error fluctuation is higher the one in the simulation case. This is due to the latency of the camera DC-motors responses to the control signal. The last two profiles in Fig. 7 are in degrees. The sudden artifacts in the pose profiles are mainly due to reading errors of the camera angles (absence of sensor-data when queried by the control software), and do not affect in any case the control performance.

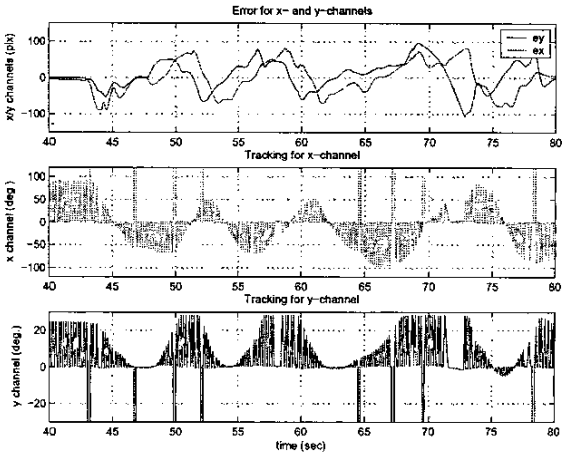


Fig. 7. Camera angles tracking using angular rate control

## VI. Conclusions

This paper presented a novel method for the design of a fuzzy gain scheduled discrete-time control that is able to deal with varying sampling-times. The design was applied to the problem of visual-servoing which is a nonlinear control problem where the varying sampling-time is due to image-processing. The results show the effectiveness of the proposed design method.

Future work will be dedicated to exploring the robustness of the system developed to both sampling-time uncertainty, unstructured uncertainties and external disturbances in actual UAV flight senarii.

## Acknowledgment

We would like to express our gratitude to the Knut and Alice Wallenberg Foundation in Sweden whose financial support made this work possible.

## References

[1] H.J. Lee, J.B. Park, G. Chen, "Robust fuzzy control of nonlinear systems with parametric uncertainties", *IEEE trans. on Fuzzy Systems*, Vol.9, num.2, Apr. 2001.

[2] H.O.Wang, K.Tanaka, *Fuzzy Control System Design and Analysis: a LMI approach* , a Wiley-Interscience Publication, John Wiley and Sons, Inc. New York, NY. 10158-0012.

[3] A. Jadbabaie, et al., "Guaranteed-cost design of Takagi-Sugeno fuzzy controllers via LMIs", *IEEE International Conference on Fuzzy Systems*, Anchorage, AK, USA, 1998.

[4] K. Tanaka et al., "Generalized Takagi-Sugeno Fuzzy Systems: Rule Reduction and Robust Control", *9th IEEE Int. Conf. on Fuzzy Systems*, vol.2, pp.688–693, San Antonio, TX-USA, May 2000.

[5] M. Sznaier, O. I. Camps, "Control issues in active-vision: Open problems and some answers2, $37^{th}$ *IEEEConference on Decisionand Control Proceedings*, Tampa, Florida, USA, 1998.

[6] P. Bergsten, M. Persson and B. Iliev, "Fuzzy gain scheduling for flight control", *IEEE Conference on Industrial Electronics, Control and Instrumentation Proceedings*, Nagoya, Japan, 2000.

[7] D. Driankov, R. Palm and U. Rehfuss, "A Takagi-Sugeno fuzzy gain scheduler", *IEEE Conference Fuzzy Systems Proceedings*, New Orleans, Florida, USA, 1996, pp. 1053–1059.

[8] P. Korba, *A gain-schedulling approach to model-based fuzzy control*, Fortschritt-Berichte VDI num.837, IBSN 3-18-383708-0, VDI Verlag GmbH, Dusseldorf, 2000.